Science of the Total Environment 740 (2020) 140149

Contents lists available at ScienceDirect

Science of the Total Environment

journal homepage: www.elsevier.com/locate/scitotenv

Sources of black carbon during severe haze events in the Beijing–Tianjin–Hebei region using the adjoint method

Yu-Hao Mao [a,b,*], Xincheng Zhao [a], Hong Liao [a,b], Delong Zhao [c], Ping Tian [c], Daven K. Henze [d], Hansen Cao [d], Lin Zhang [e], Jiandong Li [a], Jing Li [e], Liang Ran [f,g], Qiang Zhang [h]

[a] Jiangsu Key Laboratory of Atmospheric Environment Monitoring and Pollution Control/Jiangsu Collaborative Innovation Center of Atmospheric Environment and Equipment Technology, School of Environmental Science and Engineering, Nanjing University of Information Science and Technology (NUIST), Nanjing 210044, China
[b] Key Laboratory of Meteorological Disaster, Ministry of Education (KLME)/Collaborative Innovation Center on Forecast and Evaluation of Meteorological Disasters (CIC-FEMD)/International Joint Research Laboratory on Climate and Environment Change (ILCEC), NUIST, Nanjing 210044, China
[c] Beijing Weather Modification Office, Beijing 100089, China
[d] Department of Mechanical Engineering, University of Colorado, Boulder, CO 80309, USA
[e] Department of Atmospheric and Oceanic Sciences, School of Physics, Peking University, Beijing 100081, China
[f] Key Laboratory of Middle Atmosphere and global Environment Observation, Institute of Atmospheric Physics, Chinese Academy of Sciences, Beijing 100029, China
[g] Xianghe Observatory of Whole Atmosphere, Institute of Atmospheric Physics, Chinese Academy of Sciences, Xianghe 065400, China
[h] Ministry of Education Key Laboratory for Earth System Modeling, Center for Earth System Science, Tsinghua University, Beijing 100084, China

HIGHLIGHTS

- Four types of severe haze events are classified by associated synoptic weather patterns.
- Adjoint method attributes BC to sources at model spatial and temporal resolutions.
- Residential, transportation, and industry emissions are major sources to BC in BTH.
- Emissions from local and regional transport are comparable to BC at the top of PBL.
- Sources emitted in haze day and previous 2 days account for 89.8–99.3% of daily BC.

GRAPHICAL ABSTRACT

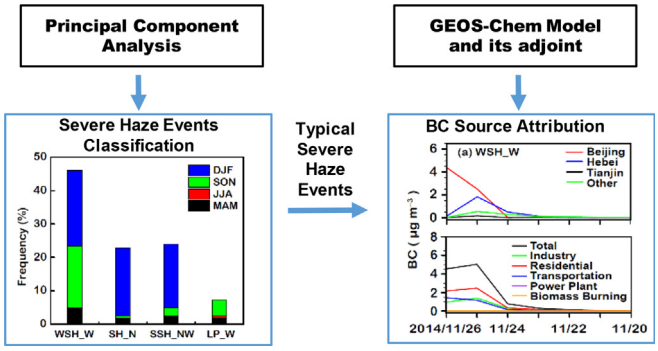

ARTICLE INFO

Article history:
Received 27 March 2020
Received in revised form 8 June 2020
Accepted 10 June 2020
Available online xxxx

Editor: Jianmin Chen

Keywords:
Black carbon
Source attribution
Severe particulate pollution in China

ABSTRACT

The Beijing-Tianjin-Hebei (BTH) region in China has been frequently suffering from severe haze events (observed daily mean surface fine particulate matter $PM_{2.5}$ concentrations larger than 150 μg m^{-3}) partially caused by certain types of large-scale synoptic patterns. Black carbon (BC), as an important $PM_{2.5}$ component and a primarily emitted species, is a good tracer for investigating sources and formation mechanisms leading to severe haze pollutions. We apply GEOS-Chem model and its adjoint to quantify the source contributions to BC concentrations at the surface and at the top of the planetary boundary layer (PBL) during typical types of severe haze events for April 2013–2017 in BTH. Four types of severe haze events, mainly occurred in December–January-February (DJF, 62.3%) and in September–October-November (SON, 26.3%), are classified based on the associated synoptic weather patterns using principal component analysis. Model results reasonably capture the daily variations of BC measurements at three ground sites in BTH. The adjoint method attributes BC concentrations to emissions from different source sectors and from local versus regional transport at the model spatial and temporal resolutions. By

* Corresponding author at: Jiangsu Key Laboratory of Atmospheric Environment Monitoring and Pollution Control/Jiangsu Collaborative Innovation Center of Atmospheric Environment and Equipment Technology, School of Environmental Science and Engineering, Nanjing University of Information Science and Technology (NUIST), Nanjing 210044, China.
E-mail address: yhmao@nuist.edu.cn (Y.-H. Mao).

https://doi.org/10.1016/j.scitotenv.2020.140149

Adjoint method
Synoptic weather patterns

source sectors, the adjoint method attributes the daily BC concentrations during typical severe haze events (in winter heating season) in Beijing largely to residential emissions (48.1–62.0%), followed by transportation (16.8–25.9%) and industry (19.1–29.5%) sectors. In terms of regionally aggregated source influences, local emissions in Beijing (59.6–79.5%) predominate the daily surface BC concentrations, while contributions of emissions from Beijing, Hebei, and outside BTH regions are comparable to the daily BC concentrations at the top of PBL (~200–400 m). Our adjoint analyses would provide a scientific support for joint regional and targeted control policies on effectively mitigating the particulate pollutions when the dominant synoptic weather patterns are predicted.

1. Introduction

China has been frequently suffering from severe particulate pollutions during recent years, particularly in the Beijing-Tianjin-Hebei (BTH) region with the rapid industrialization and urbanization (Li et al., 2019; L. T. Wang et al., 2014; Y. Wang et al., 2014). Although the frequency of severe haze days (observed daily mean surface fine particulate matter $PM_{2.5}$ concentrations larger than 150 μg m^{-3}) has been decreasing because of the Chinese Air Pollution Prevention and Control Action Plan released in 2013, observed daily surface $PM_{2.5}$ concentrations in BTH can still reach 500 μg m^{-3} due to large anthropogenic emissions (e.g., S. X. Wang et al., 2014) and unfavorable meteorological conditions (e.g., Li et al., 2018; Li et al., 2019). Understanding sources of particulate pollution is thus essential for emission control strategies and air quality planning in China.

Black carbon (BC), as an important $PM_{2.5}$ component, has considerable impacts on air quality and human health (e.g., Anenberg et al., 2011; Smith et al., 2009). Because of its strong absorption of solar radiation, BC acts as the third largest contributor to climate change (e.g., IPCC, 2013; Ramanathan and Carmichael, 2008). It has been proposed that BC reduction may immediately slow down the global warming and simultaneously improve air quality and public health (Anenberg et al., 2012; Bond et al., 2013; Shindell et al., 2012). The observed annual mean BC concentrations in BTH are more than 5 μg m^{-3} (Chen et al., 2016; X. Y. Zhang et al., 2012) and daily BC concentrations in severe particulate pollution episodes can exceed 30 μg m^{-3} (e.g., Jin et al., 2014; Wu et al., 2016). Previous studies have shown that BC enhances the occurrences of severe haze pollution events through the "dome effect" (Ding et al., 2016). The existence of BC induces heating in the upper planetary boundary layer (PBL) and resulting decreases surface heat flux and substantially depresses the development of PBL (Ding et al., 2016; Liao and Liao, 2014; Wendisch et al., 2008). BC is a primarily emitted species and thus a good tracer to understand the sources and formation mechanisms leading to severe particulate pollutions.

Previous modeling studies on BC source attribution in China are mainly based on back-trajectory receptor models (e.g., Lu et al., 2012; Y. Wang et al., 2017; Zhang et al., 2013; X. Zhang et al., 2015; Zheng et al., 2019), tagged tracer/region method (e.g., Chen et al., 2015; J. Li et al., 2016; Wang et al., 2015; Yang et al., 2017), or sensitivity simulations with perturbed emissions using a chemical transport model (CTM) (e.g., K. Li et al., 2016; L. T. Wang et al., 2014). Back-trajectory method can generally reliably attribute sources on continental scales as model integration error enlarges with modeling time increased (D. Liu et al., 2015). Tagged tracer and sensitivity simulations are computationally limited in the numbers of emission sectors and source regions and thus require unaffordable computational time. The adjoint model offers a computationally efficient method to attribute sources of chemical species at the spatial and temporal resolutions of the CTM (Henze et al., 2007, 2009). A single run of the adjoint model can compute the sensitivity of aerosol concentrations at a receptor site (or an average over a region) and time (or an average over a time period) to global emissions at the CTM resolution (Qi et al., 2017; L. Zhang et al., 2015).

A number of studies have shown that certain types of large-scale synoptic patterns would easily cause the formation and maintaining of severe particulate pollutions in BTH (Li et al., 2019; Miao et al., 2017; J. P. Zhang et al., 2012; Y. Zhang et al., 2016). To our knowledge, few studies have systematically examined BC source attribution in BTH during different types of severe haze events classified by the associated synoptic weather patterns. Here we apply the GEOS-Chem model and its adjoint to interpret the BC sources in BTH during the typical types of severe haze events. We classify the typical severe haze events based on associated synoptic weather patterns using principal component analysis (Li et al., 2019; Miao et al., 2017; J. P. Zhang et al., 2012). The adjoint method then attributes the daily BC concentrations at the surface and at the top of the PBL in BTH during typical severe haze events to emissions from different source sectors and from local versus regional transport at the model spatial and temporal resolutions. Targeted emission control measures thus can be implemented when the dominant synoptic weather patterns are predicted.

2. Methods

2.1. GEOS-Chem and its adjoint

The GEOS-Chem global 3-D CTM is driven by assimilated meteorology from the Goddard Earth Observing System (GEOS) of the NASA Global Modeling and Assimilation Office (GMAO) (Bey et al., 2001). Here we use GEOS-Chem version 8-02-01 and its adjoint model version 35 (available at http://geos-chem.org) driven by the GEOS-FP assimilated data with a temporal resolution of 3 h (1 h for surface variables and mixing depths) and a horizontal resolution of 0.25° × 0.3125°. This fine resolution may better represent the heterogeneity in topography and emissions over BTH and improve the model simulations of urban air pollution discussed in the present study (L. Zhang et al., 2015, 2016). Following our previous BC modeling studies (Mao et al., 2015, 2016, 2017), we conduct 'offline' simulations of carbonaceous aerosols for computational expediency during October 2012–2017 at both 2° × 2.5° (globally) and 0.25° × 0.3125° (nested over Eastern Asia, 60°–150°W longitudes, −11°–55°N latitudes) horizontal resolutions. The first three months are used for initialization. The detailed model parameterizations for BC simulation are discussed by Mao et al. (2016).

The global monthly anthropogenic emissions of BC are from the Hemispheric Transport of Air Pollution (HTAP, http://edgar.jrc.ec.europa.eu/htap_v2/index.php? SECURE = 123, Janssens-Maenhout et al., 2015) for 2010. We update the monthly anthropogenic BC emissions in China with the Multi-Resolution Emission Inventory (MEIC, Zheng et al., 2018) of China at 0.5° × 0.667° horizontal resolution. BC emissions of MEIC are available for 2013–2017 and includes four anthropogenic emission sectors (residential, industry, transportation, and power plant). We summarize the annual emission inventories of BC in China in Table 1, which shows that residential, industry, and transportation are three major emission sectors in China, accounting for 48.2–52.2%, 25.5–34.8%, and 16.9–24.4% of annual total anthropogenic BC emissions, respectively. The contributions from power plant are less than 3% in different emission inventories. For MEIC emission inventory, the emissions from power plant in China only account for less than 0.1% of the total anthropogenic emissions. Under the strict emission

Table 1
Summary of annual BC emission inventories in China (Gg C yr^{-1}). Values in the parentheses (%) are the relative contributions from individual emission sectors to total BC emissions.

Reference	Year	Industry	Residential	Transportation	Power plant	Biomass burning	Total
This work	2013	608 (34.8)	841 (48.2)	294 (16.9)	2 (0.1)	59 (3.3)	1804
MEIC	2014	523 (32.7)	791 (49.5)	284 (17.7)	1 (0.1)	85 (5.0)	1684
GFEDv4	2015	424 (29.3)	748 (51.5)	277 (19.1)	1 (0.1)	76 (5.0)	1526
	2016	348 (26.5)	686 (52.2)	278 (21.2)	1 (0.1)	53 (3.9)	1366
	2017	319 (25.5)	626 (50.0)	306 (24.4)	1 (0.1)	57 (4.3)	1309
HTAP	2010	550 (31.8)	893 (51.6)	270 (15.6)	18 (1.0)	N.A.	1731
Lu et al. (2011)	2010	501 (27.1)	936 (50.6)	283 (15.3)	21 (1.1)	109 (5.9)	1850
	2008	510 (28.6)	888 (49.7)	259 (14.5)	19 (1.1)	110 (6.1)	1786
Qin and Xie (2012)	2009	735 (39.1)	777 (41.3)	241 (12.8)	11 (0.6)	117 (6.2)	1881
Wang et al. (2012)	2007	646 (33.1)	988 (50.7)	188 (9.6)	51 (2.6)	78 (4.0)	1951
Zhang et al. (2009)	2006	575 (31.8)	1002 (55.3)	198 (10.9)	36 (2.0)	N.A.	1811

reduction measures, the annual BC emissions in China from MEIC decrease from 1.74 Tg C in 2013 to 1.25 Tg C in 2017. The decreasing trend in anthropogenic BC emissions is largely due to the decreasing emissions in residential and industrial sectors. Compared with previous anthropogenic BC emission inventories in China in Table 1, emissions from the residential and industry sectors decrease significantly in MEIC while those from transportation sector increase. The BTH is one of the highest BC emission regions in China, accounting for ~15% of the China's annual total BC emissions (Fig. S1). The anthropogenic BC emissions in BTH are mainly from residential (41.9%), industry (37.0%), and transportation (21.0%) emission sectors in MEIC averaged for 2013–2017. The contributions from power plant in BTH are less than 0.1% in MEIC. The annual total anthropogenic BC emissions in the BTH region decrease by 39% from 2013 to 2017 (Fig. 1). The corresponding industry and residential emissions of BC in BTH decrease by 54.3% and 40.8%, respectively, while emissions from transportation sector show a slight increase by 1.3%.

Biomass burning emissions of BC are taken from the Global Fire Emissions Database version 4 (GFEDv4; van der Werf et al., 2017) with a monthly temporal resolution. The annual biomass burning emissions of BC are 53.0–84.6 Gg C in China and 1.8–2.1 Gg C in BTH for 2013–2017, accounting for 3.3–5.0% of total BC emissions in China and ~1.0% in BTH (Figs. 1 and S1). Previous studies (Fu et al., 2012; M. Liu et al., 2015; Yin et al., 2019) have pointed out that biomass burning emissions retrieved from satellite burnt area data, such as GFED, are significantly underestimated the seasonal agriculture waste burning in northern China, especially in early summer.

We use the GEOS-Chem adjoint model to attribute BC sources in BTH. The GEOS-Chem adjoint model has been validated and applied in source attribution of chemical species and emission optimization in a number of studies (e.g., Kopacz et al., 2011; Mao et al., 2015; Qi et al., 2017; L. Zhang et al., 2015, 2016). The adjoint model provides a computationally efficient approach to calculate the sensitivity of aerosol concentrations (e.g. BC concentrations at a given site) to global emissions

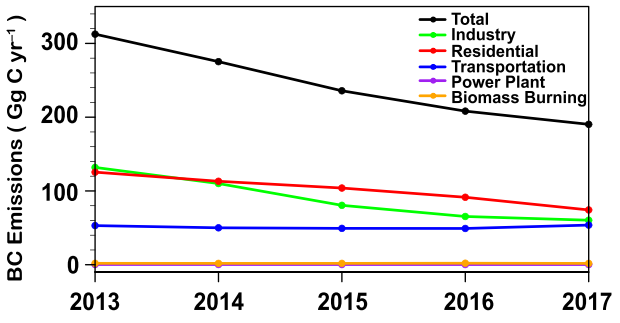

Fig. 1. Annual BC emissions (Gg C yr^{-1}) in Multi-Resolution Emission Inventory (MEIC) from four anthropogenic emission sectors (residential, industry, transportation, and power plant) and in Global Fire Emissions Database version 4 (GFEDv4) in Beijing–Tianjin–Hebei for 2013–2017.

at the spatial and temporal resolutions of the model (e. g. BC emissions at 0.25° × 0.3125° horizontal resolution and hourly temporal resolution) simultaneously backwards in time. The detailed introduction of GEOS-Chem adjoint model are discussed by Henze et al. (2007, 2009) and L. Zhang et al. (2015).

2.2. Observations

Previous validations have shown that the GEOS-Chem model can reasonably capture the decadal, interannual, and seasonal variations of BC concentrations in China (Fu et al., 2012; K. Li et al., 2016; Mao et al., 2016). We further evaluate the ability of GEOS-Chem model to simulate the day-to-day variations of BC concentrations in BTH by using ground-based measurements of daily BC concentrations at two urban stations: Beijing Weather Modification Office (BWMO, 39.94°N, 116.28°E, 30 m) for 2013–2014 and for August 2016–2017 and Peking University (PKU, 39.99°N, 116.31°E, 55 m) for August–December 2017 (Chang et al., submitted), and also at one rural site Xianghe (XH, 39.80°N, 116.96°E, 35 m) in Hebei province for February 2013–March 2015 (Ran et al., 2016). The locations of the sites are shown in Fig. S2. Aerosol absorption coefficients are measured every 5 min at 880 (532) nm at BWMO and XH (PKU) stations by Magee Aethalometer, based on the changes in optical attenuation before and after the atmospheric aerosol collected. BC mass concentrations are then directly converted from aerosol absorption coefficients using the mass absorption cross section of 16.6 (8.28) $m^2\ g^{-1}$ at BWMO and XH (PKU) stations and corrected for the loading effect.

$PM_{2.5}$ concentrations used in this study (shown in Fig. S2) are measured based on the micro-oscillating balance method and the β absorption method by Ministry of Ecology and Environment of China (available from: http://106.37.208.233:20035/), which have been widely investigated to understand the particulate pollution in China (Song et al., 2017; J. D. Wang et al., 2017; Y. G. Wang et al., 2014; Zhang and Cao, 2015). There are 78 sites in the BTH region with hourly measurements of surface $PM_{2.5}$ concentrations, which are available from April 2013. The daily mean surface $PM_{2.5}$ concentration at each site is calculated only when more than 20 h of valid observations are available during that day.

2.3. Classification of synoptic weather patterns for severe haze events

The obliquely rotated principal component analysis in the T-mode (T-PCA, Huth, 2000) has been proved to be a reliable classification method to investigate the synoptic weather patterns for the haze events in China (Li et al., 2019; Miao et al., 2017; Xu et al., 2016; J. P. Zhang et al., 2012). The principle of T-PCA is to calculate eigenvectors of the input data by singular value decomposition for classifying typical patterns (Miao et al., 2017). We use in the present study the cost733 software package (http://cost733.met.no) of T-PCA to classify the prevailing circulation patterns during the severe haze events in BTH for April 2013–2017. The input data are sea level pressure and geopotential

height at the 500 hPa and 850 hPa levels in eastern Asia (20–70°N, 70–130°E) with a horizontal resolution of 0.25° × 0.25° and a temporal resolution of 6 h obtained from the European Centre for Medium-Range Weather Forecasts, ERA5 datasets (ECMWF, https://cds.climate.copernicus.eu/cdsapp#!/search?type=dataset).

3. Simulated BC and model evaluation

We have systematically evaluated the performance of GEOS-Chem model in BC simulations in China (K. Li et al., 2016; Mao et al., 2016). Simulated BC concentrations in China are likely underestimated because of coarse resolution of the CTM and the biased low anthropogenic emissions (e.g., Bond et al., 2013; Fu et al., 2012; Mao et al., 2016). In Fig. 2, we further evaluate the ability of the GEOS-Chem model to capture the daily variations of BC in BTH. To compare with observations, model results are sampled at the corresponding locations of the stations and the periods when the measurements are available. The correlation coefficients between observed and simulated daily BC concentrations are 0.58 at BWMO for 2013–2014 and for August 2016–2017, 0.61 at PKU for August–December 2017, and 0.40 at XH for February 2013–March 2015. Compared to observations, GEOS-Chem simulated BC concentrations are biased low by −1% at PKU, −23.3% at BWMO, and −26.9% at XH. The bias in the present model results is smaller than the low biases from previous GEOS-Chem studies, i.e., Fu et al. (2012), K. Li et al. (2016), and Mao et al. (2016). The fine resolution model and latest emission inventory used in the present study likely improve the model versus observation comparisons.

Fig. 3 shows the scatter plots of simulated and observed daily BC concentrations at three stations for each season. Model performance is further evaluated by the seasonal correlation coefficients between model results and observations. The seasonal correlation coefficients are within the range of 0.30–0.59 at BWMO, 0.52–0.72 at PKU and 0.36–0.51 at BWMO. Model performance is best in December–January-February (DJF) with correlation coefficients ranging from 0.51 to 0.72 and is worst in June–July-August (JJA) with the correlation coefficients from 0.30 to 0.52. All the correlation coefficients are statistically significant with 95% confidence from a two-tailed Student's *t*-test. The better model performance at the two rural sites in DJF when anthropogenic emissions dominated implies that the MEIC anthropogenic emissions prescribed in the model appear to be acceptable. The poor correlations in JJA thus can be partially attributed to the biomass burning emissions of BC being underestimated in the model, especially in rural regions. The severely underestimated agricultural waste burning in GFEDv4 in early summer is likely a large seasonal source in northern China (M. Liu et al., 2015; Yin et al., 2019).

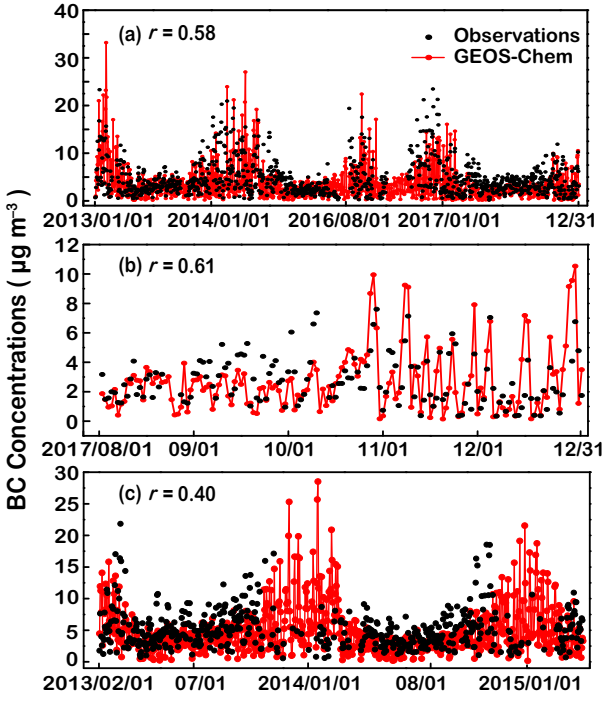

Fig. 2. Observed (black) and simulated (red) daily surface BC concentrations (μg m^{-3}) at (a) Beijing Weather Modification Office station for 2013–2014 and for August 2016–2017, (b) Peking University station for August–December 2017, and (c) Xianghe station for February 2013–March 2015. Also shown are the correlation coefficients (*r*) between observed and simulated BC concentrations. (For interpretation of the references to colour in this figure legend, the reader is referred to the web version of this article.)

4. Dominant synoptic weather patterns of severe haze events in BTH

The severe haze days are defined in the present study as observed daily mean surface $PM_{2.5}$ concentrations larger than 150 μg m^{-3} following the previous studies (Cai et al., 2017; Li et al., 2019). For classification of typical circulation patterns, we examine 167 large-scale severe haze events when more than 6 cities in BTH (13 cities in total) experienced severe particulate pollution from April 2013 to 2017. The frequencies of the severe haze days (Fig. 4) are 62.3% in DJF, 26.3% in September–October-November (SON), and 10.8% in March–April-May (MAM). We use T-PCA classification method to categorize the corresponding synoptic weather patterns of the 167 severe haze days to four dominant types for the region. Types WSH_W (weak Siberian High in the west), SH_N (Siberian High in the north), and SSH_NW (strong Siberian High in the northwest) are the dominant synoptic weather patterns in BTH, accounting 46.1%, 22.8%, and 23.9% of the severe haze days, respectively. Type LP_W (low pressure system in the west of BTH) is only responsible for 7.2%.

Fig. 5 shows the sea level pressure and 10 m wind field, as well as the geopotential height and corresponding wind field at 850 hPa and 500 hPa levels for the four typical large-scale synoptic patterns. In type WSH_W, the dominant seasons for the severe haze days are DJF (49.4%) and SON (40.3%). The Siberian High is weak and high pressure centers on Xinjiang autonomous region. Eastern China is controlled by the uniform pressure and thus weak pressure gradients and relatively weak winds, which are favorable for the accumulation of haze pollutions. In type SH_N, the frequency of the severe haze days is highest in DJF (89.5%). The central pressure of the relatively strong Siberian High is about 1056 hPa. The cold high locates over Mongolia, moves eastward, and passes through northern China. Eastern China is located in the southern part of this cold high. In type SSH_NW, 80.0% of severe haze days occur in DJF. The cold high originates in Siberia and moves toward southeast. The Siberian High is stronger than that in SH_N, with a central pressure of 1064 hPa extends to northeastern China. SON accounts for 66.7% of the severe haze days in type LP_W. The Siberian cold high is extremely weak and has few influences on eastern China. Eastern China is influenced by a weak high centered over the Sea of Japan and a low pressure centered over Mongolia, which lead to southerlies in BTH.

In WSH_W, SH_N, and SSH_NW three dominant circulation types, severe haze events are most frequent in DJF and BTH is controlled by relatively week winds, mostly westerlies, southerlies, and sometimes easterlies, which are not conducive to pollution diffusion in the region and might easily lead to the high aerosol concentrations. The simulated daily surface BC concentrations in Beijing are 8.3 μg m^{-3} in WSH_W, 7.5 μg m^{-3} in SH_N, and 8.9 μg m^{-3} in SSH_NW, respectively, averaged for each type of large-scale severe haze events in DJF. The corresponding values in SON are 5.8, 3.6, and 6.5 μg m^{-3}, respectively. Those values in severe haze events are much higher than the seasonal mean of simulated daily surface BC concentrations in Beijing, which are only 5.0 μg m^{-3} DJF and 3.5 μg m^{-3} in SON.

All four circulation types show some similar patterns at 850 and 500 hPa, consistent with those reported by Li et al. (2019), which

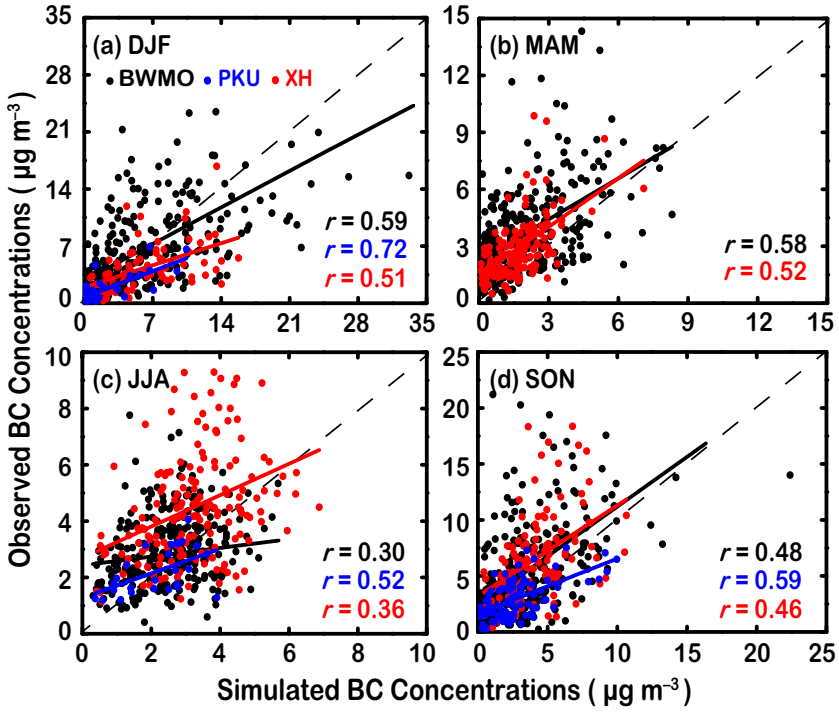

Fig. 3. Simulated versus observed daily surface BC concentrations (μg m^{-3}) at three stations (circles) and reduced-major axis regression lines (solid lines) for each season. Black: Beijing Weather Modification Office station (BWMO) for 2013–2014 and for August 2016–2017; Blue: Peking University station (PKU) for August–December 2017; Red: Xianghe station (XH) for February 2013–March 2015. Also shown are correlation coefficients (r) between observed and simulated BC concentrations for each season. Dashed lines indicate 1:1 line. (For interpretation of the references to colour in this figure legend, the reader is referred to the web version of this article.)

favor the formation and maintenance of severe haze pollutions. An anticyclone located over the East China Sea at 850 hPa (Fig. 5b) leads to the southerlies in eastern China; a weak East Asia trough at 500 hPa (Fig. 5c) induces the relatively weak meridional winds and westerlies prevailing in northern China.

According to the T-PCA classification results, we select typical severe haze days for source attribution based on the following two criterions: (1) the synoptic weather pattern remains the same type for more than four consecutive days previous to each selected day; (2) measurements are available in the selected days and the differences between the observed and simulated daily surface BC concentrations are within ± 20%. Three typical severe haze days are thus selected for source analysis hereinafter: November 26, 2014 (WSH_W), December 16, 2013 (SH_N), and February 15, 2014 (SSH_NW). Fig. S3 compares the sea level pressure and 10 m wind field from ERA5 for identifying prevailing synoptic types and from GEOS-FP for driving GEOS-Chem model. For each selected severe haze event, the circulation patterns in the two reanalysis data show the similar meteorological characteristics, which are also generally consistent with the corresponding type of averaged synoptic patterns shown in Fig. 5a.

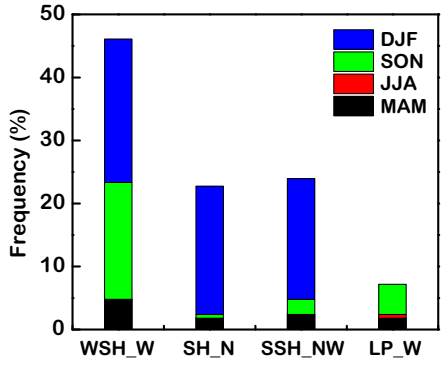

Fig. 4. Seasonal frequency (%) of four types of severe haze days in Beijing–Tianjin–Hebei for April 2013–2017. Four types of synoptic weather patterns are WSH_W (weak Siberian High in the west), SH_N (Siberian High in the north), SSH_NW (strong Siberian High in the northwest), and LP_W (low pressure system in the west of BTH).

5. Sources of BC in typical severe particulate events

Fig. 6 shows the contributions from four anthropogenic emission sectors (residential, transportation, industry, and power plant) and biomass burning emissions to daily surface BC concentrations in Beijing (the grid cell covering the center of Beijing: 39.99°N, 116.31°E, open star in Fig. S2) on three typical severe haze events, November 26, 2014 (WSH_W), December 16, 2013 (SH_N), and February 15, 2014 (SSH_NW). The contributions are integrated backward for one week from the severe haze days as computed by the GEOS-Chem adjoint model at 0.25° × 0.3125° horizontal resolution and hourly temporal resolution. The total values summed up over the model domain (Fig. 6 left panel) approximate (differences within ±10%) the daily surface BC concentrations from forward model simulations in Beijing on the severe haze days. Daily contributions from local and regional influences and from different emission sectors are shown in Fig. 7. We further summarize in Table 2 the relative contributions integrated backward for one week to daily BC concentrations in Beijing on the severe haze days. Fig. S4 shows the BC emissions (Gg C) in MEIC and in GFEDv4 for the month when each selected haze event occurs.

In terms of regionally aggregated source influences (Fig. 7 left panel), local emissions in Beijing predominate (by 59.6–79.5%) the daily surface BC concentrations on three severe haze days. Emissions in Hebei and Tianjin provinces account for 12.7–24.2% and 1.8–5.1%, respectively. The geographical distribution of adjoint sensitivity indicates pollution transport from regions outside BTH (Fig. 6). The sources over Shanxin and northwestern of Shandong provinces contribute about 9.9% in type WSH_W. In type SH_N, sources outside BTH only contribute

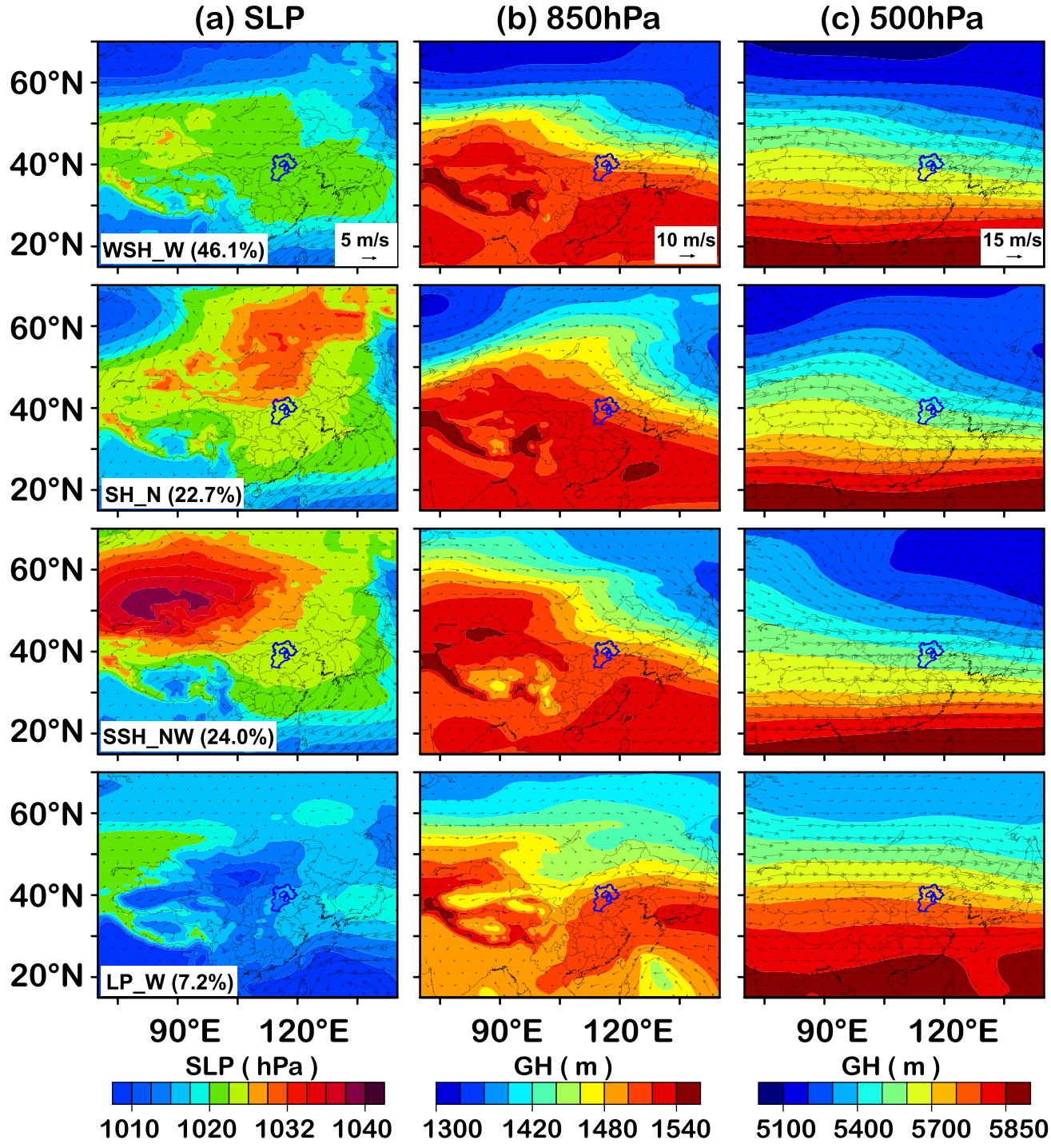

Fig. 5. Synoptic weather patterns for severe haze days in Beijing–Tianjin–Hebei for April 2013–2017. (a) sea level pressure (SLP, hPa) and wind field (m s^{-1}) at 10 m, (b) geopotential height (GH, m) and wind field at 850 hPa, and (c) geopotential height and wind field at 500 hPa. Four types of synoptic weather patterns are WSH_W (weak Siberian High in the west), SH_N (Siberian High in the north), SSH_NW (strong Siberian High in the northwest), and LP_W (low pressure system in the west of BTH).

4.1% of daily surface BC concentrations, mainly in Shandong and Inner Mongolia provinces. Sources in four provinces around BTH (Shandong, Henan, Shanxin, and Inner Mongolia provinces) account for 13.7% in type SSH_NW. The geographical distribution pattern of source contribution to daily BC concentrations for each severe haze event is consistent with the corresponding 10 m wind field in BTH shown in Fig. S3. Our results are generally consistent with those from L. Zhang et al. (2015), which used the GEOS-Chem model (at 0.25° × 0.3125° horizontal resolution) and its adjoint and MEIC emissions for year 2010 to attribute the surface $PM_{2.5}$ over northern China to sources from different source sectors and source regions for January of 2013–2015. The estimated surface $PM_{2.5}$ concentrations in Beijing during January 2013–2015 were largely impacted by local emissions (52.8%), and considerably influenced by sources in Hebei (26.1%) and Tianjin (6.7%) provinces and sources transported further away (14%).

By emissions sectors (Fig. 7 right panel), residential sources (48.1–58.9%) are the major emission sector contributing to daily surface BC concentrations in Beijing during severe haze days, followed by emissions from transportation sector (20.8–25.9%) and industry (19.1–25.9%). For local sources in Beijing, transportation sector accounts

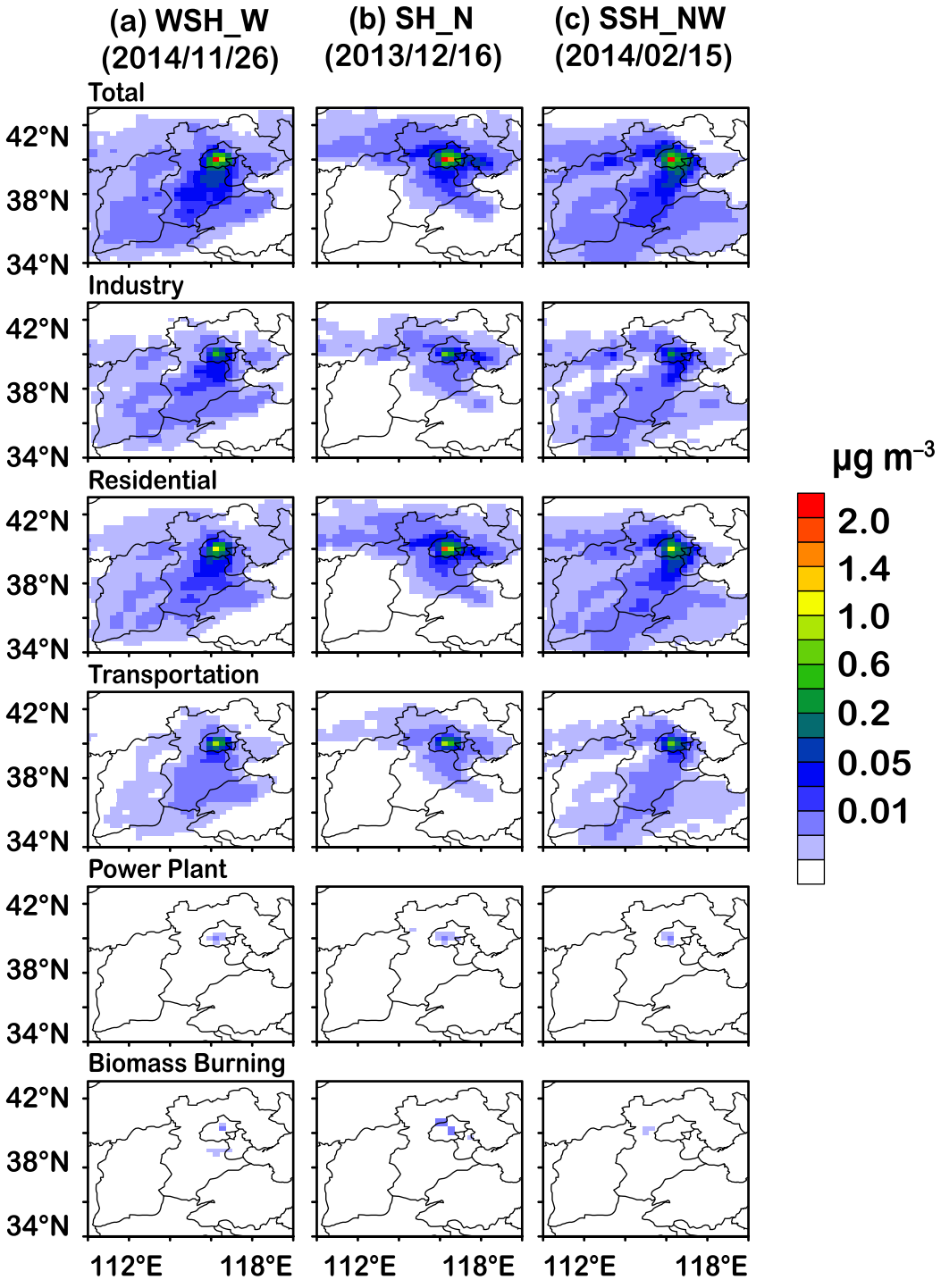

Fig. 6. Contributions to daily surface BC concentrations (μg m^{-3}) in Beijing on three typical severe haze days from four anthropogenic emission sectors (residential, industry, transportation, and power plant) and biomass burning emissions, computed by the GEOS-Chem adjoint model integrated over (a) November 10–16, 2014 (type WSH_W, weak Siberian High in the west), (b) December 10–16, 2013 (type SH_N, Siberian High in the north), and (c) February 9–15, 2014 (type SSH_NW, strong Siberian High in the northwest).

for 15.7–20.0% of daily surface BC concentrations on severe haze days, and is thus more important than local industry sources (9.4–13.5%). For sources of regions outside Beijing, the contributions from industry emissions (5.6–17.8%) are larger than those from transportation sector (2.2–5.9%). The contributions from power plant are less than 0.1% of daily surface BC concentrations on severe haze days in Beijing.

The uncertainties exist in source attribution of BC concentrations during the severe haze events, partially due to the discrepancies between GEOS-Chem simulated and observed BC concentrations. Other possible reasons include large uncertainties in both anthropogenic and biomass burning emissions and also changes of emissions in different seasons and in different years. During the winter heating season (November–March) in BTH, residential emissions account for 56.2% of total anthropogenic emissions averaged for 2013–2017, and thus become the dominant contributor to the daily surface BC concentrations in the three selected severe haze events. For non-heating season (April–October), monthly averaged residential emissions are only 27.7% of those in heating season and 25.3% of total anthropogenic emissions. The sources from industry and transportation sectors in non-heating season are 48.0% and 26.7% of total anthropogenic emissions.

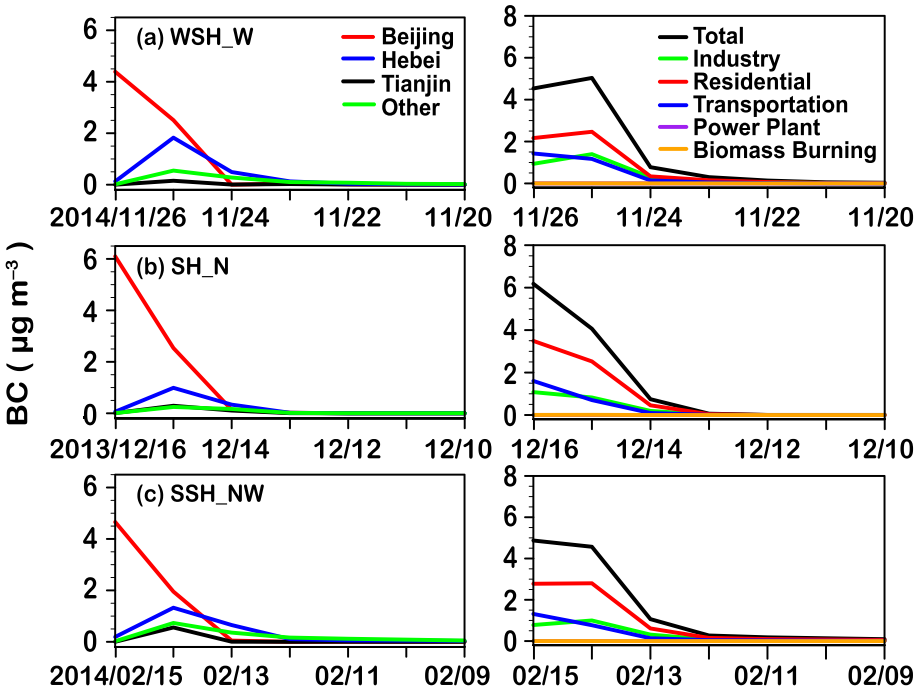

Fig. 7. Time-dependent daily contributions to daily surface BC concentrations (μg m^{-3}, going backward for one week and integrating over every 3 h) in Beijing: (left) from Beijing, Tianjin, and Hebei three provinces and the regions outside Beijing–Tianjin–Hebei; (right) from four anthropogenic emission sectors and biomass burning emissions integrated over the model domain. Results are computed by the GEOS-Chem adjoint model for three typical severe haze events: (a) November 16, 2014 (type WSH_W, weak Siberian High in the west), (b) December 16, 2013 (type SH_N, Siberian High in the north), and (c) February 15, 2014 (type SSH_NW, strong Siberian High in the northwest).

It is therefore inferred that the contribution from industry, residential, and transportation sectors would be comparable to daily BC concentrations during severe haze events in non-heating season (early autumn and late spring). For severe haze events during more recent years, the contribution from residential sector to BC concentrations is likely smaller than those during the selected haze events in 2013 and 2014, as the significant reduction of residential emissions in MEIC from 2013 to 2017.

Our previous study by K. Li et al. (2016) used sensitivity simulations to quantify the contributions from different source sectors to surface BC in China for 2010 by the GEOS-Chem model at 0.5° × 0.667° horizontal resolution and with HTAP emissions. Compared with the results from K. Li et al. (2016) and L. Zhang et al. (2015), the contributions from transportation sector are much larger in the present study while those from residential and industry sources are smaller, largely because of the higher emissions in transportation sector in MEIC but lower in

Table 2
Relative contributions (%) to daily BC concentrations at the surface and at the top of the planetary boundary layer in Beijing on three typical severe haze days from three anthropogenic emission sectors and from local and regional influences, computed by the GEOS-Chem adjoint model integrated over November 20–26, 2014 (type WSH_W, weak Siberian High in the west), December 10–16, 2013 (type SH_N, Siberian High in the north), and February 9–15, 2014 (type SSH_NW, strong Siberian High in the northwest). Relative contributions from power plant and biomass burning emissions are less than 0.1% and 0.2%, respectively, and thus not included.

		WSH_W 2014/11/26		SH_N 2013/12/16		SSH_NW 2014/02/15	
		Surface	High	Surface	High	Surface	High
Beijing	Total	64.1	42.2	79.5	61.9	59.6	35.9
	Residential	30.9	21.1	46.2	38.1	34.5	21.5
	Transportation	20.0	12.4	19.6	13.5	15.7	8.7
	Industry	13.1	8.7	13.5	10.1	9.4	5.7
Tianjin	Total	1.8	1.9	3.7	5.3	5.1	7.7
	Residential	0.9	1.0	2.4	3.3	3.3	5.0
	Transportation	0.3	0.3	0.4	0.5	0.6	0.9
	Industry	0.6	0.6	1.0	1.4	1.2	1.8
Hebei	Total	24.2	39.1	12.7	23.7	21.5	33.4
	Residential	11.7	18.8	7.9	15.2	13.6	21.0
	Transportation	4.3	6.9	1.4	2.6	2.8	4.4
	Industry	8.2	13.4	3.4	5.9	5.1	8.1
Outside Beijing-Tianjin-Hebei	Total	9.9	16.7	4.1	9.2	13.7	23.0
	Residential	4.5	7.7	2.4	5.5	7.3	12.3
	Transportation	1.4	2.3	0.4	0.9	1.7	2.9
	Industry	4.0	6.8	1.2	2.8	4.7	7.9
Total	Residential	48.1	48.6	58.9	62.0	58.7	59.7
	Transportation	25.9	21.8	21.8	17.5	20.8	16.8
	Industry	25.9	29.5	19.1	20.2	20.4	23.5

residential and industry during recent five years. With an increased ratio of the transportation sector in the total anthropogenic emissions, the contributions from transportation sector to BC concentrations likely keep growing.

Biomass burning emissions account for less than 0.2% of daily surface BC concentrations during three severe haze events, as biomass burning emissions are only 0.2% of total BC emissions in heating season in BTH. In early summer, biomass burning emissions account for up to 4.1% of total BC emissions in the region and thus become a larger contributor to BC concentrations. Our estimates of the contribution of biomass burning emissions are likely underestimated due to severely missing agricultural waste burning in GFEDv4 in northern China (M. Liu et al., 2015; Yin et al., 2019). Our previous study by K. Li et al. (2016) used biomass burning emissions from Lu et al. (2011) and also showed that biomass burning emissions largely from agricultural waste burning may account for 9% of surface BC concentrations in the North China Plain in the SON harvest season for 2010.

Daily surface BC concentrations during haze events are most sensitive to sources from the pollution days and their previous 2 days. The source accumulations in the 3-day periods account for 95.2% of daily BC concentrations on November 26, 2014 (WSH_W), 99.3% on December 16, 2013 (SH_N), and 93.9% on February 15, 2014 (SSH_NW). Surface BC is most sensitive to local sources in Beijing within 2 days prior to reaching the receptor site. The Tianjin and Hebei emissions take about 0–3 days of transport to impact the surface BC in Beijing on the haze days. Contribution maxima appear on the pollution days for local sources in Beijing and on the previous one day for emissions in Tianjin and Hebei. Emissions outside BTH transport 0–5 days before arriving at Beijing.

Previous studies have shown that BC in the upper PBL favors the formation of the inversion layer and depresses the PBL development, and thus increases the occurrences and durations of severe haze pollutions (Ding et al., 2016; Liao and Liao, 2014; Wendisch et al., 2008). We thus further analyze the daily contributions from four anthropogenic emission sectors and from local and regional influences (Fig. 8) to daily BC concentrations at the top of the PBL in Beijing during three typical severe haze days. The daily averaged PBL heights are about 200–400 m in the three severe haze days. The relative contributions integrated backward for one week are summarized in Table 2. For emission sectors (Fig. 8 right panel), residential sources (48.6–62.0%) again are the major contributor to daily BC concentrations at the top of the PBL in Beijing during severe haze days, followed by emissions from transportation sector (16.8–21.8%) and industry (20.2–29.5%).

By regions (Fig. 8 left panel), local emissions in Beijing (35.9–61.9%) and emissions in Hebei (23.7–39.1%) are the predominate sources to the daily BC concentrations at the top of the PBL on the severe haze days, followed by sources outside BTH (9.2–23.0%) and in Tianjin (1.9–7.7%). Local emissions in Beijing are more sensitive to BC concentrations at the surface while emissions in Hebei and outside BTH are more important to BC concentrations at the top of the PBL. The source accumulations on the pollution days and their previous 2 days account for 89.8–98.8% of daily BC concentrations. Contribution maxima appear one day previous the pollution days; the sources in Beijing and Hebei show the largest daily influences by 21.2–38.5% and 16.3–25.0%, respectively. The emissions in Tianjin and Hebei transport 0–3 days before arriving at Beijing and contributions from emissions outside BTH show a longer tail (~two day time lag).

6. Summary and conclusions

This present study systematically quantified the source contributions to BC concentrations during the typical types of severe haze events in BTH for 2013–2017 using the GEOS-Chem model and its adjoint. The GEOS-Chem model were driven by the GEOS-FP assimilated data with fine model horizontal resolution (0.25° × 0.3125°) and the MEIC anthropogenic emission inventory in China. We evaluated simulated daily mean surface BC concentrations by ground-based measurements of BC concentrations at the three stations in BTH. The GEOS-Chem model reasonably captured the daily variations of observed surface BC concentrations in BTH. The seasonal correlation coefficients between observed and simulated daily surface BC concentrations were within the ranges of 0.51–0.72 in DJF and 0.30–0.52 in JJA, indicating that MEIC anthropogenic emissions of BC were acceptable prescribed in the model while biomass burning emissions in GFEDv4 were likely underestimated due to severely missing agricultural waste burnings.

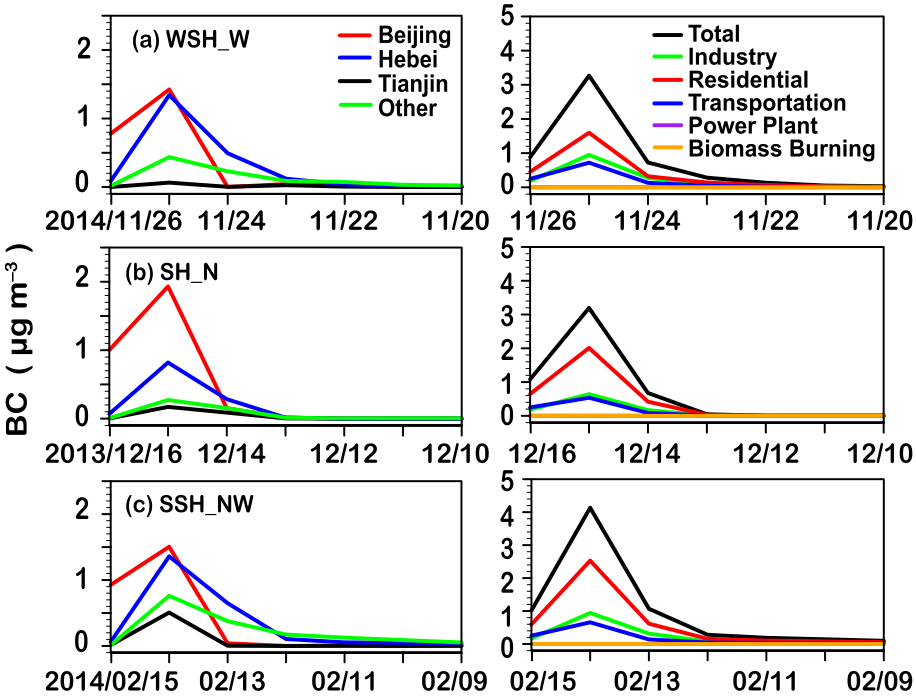

Fig. 8. Same as Fig. 7, but for contributions to daily BC concentrations at the top of the planetary boundary layer.

We also applied T-PCA method by using the sea level pressure and geopotential height data from the ECMWF ERA5 to classify the prevailing circulation patterns during the severe haze events. Four dominant types of synoptic weather patterns were identified in BTH for April 2013–2017, with the largest frequencies of the severe haze days in DJF (62.3%) and SON (26.3%). Types WSH_W, SH_N, and SSH_NW were the dominant weather patterns in BTH, accounting for 46.1%, 22.8%, and 24.0% of severe haze days, respectively. In three dominant circulation types, BTH was controlled by relatively week winds, mostly westerlies, southerlies, and sometimes easterlies, which would easily lead to the high aerosol concentrations in the region.

The adjoint method attributed BC concentrations at the surface and at the top of the PBL to emissions from different source sectors and from local versus regional transport at the model spatial and temporal resolutions. Adjoint analyses showed that residential (48.1–62.0%) was the major emission sector contributing to daily BC concentrations in Beijing during severe haze days in winter heating season, followed by transportation sector (16.8–25.9%) and industry sector (19.1–29.5%). For local emissions in Beijing, sources from transportation sector (8.7–20.0%) were more important than industry emissions (5.7–13.5%); for sources outside Beijing, the contributions from industry emissions (5.6–20.8%) were larger than those from transportation sector (2.2–9.4%).

By source influences summed by regions, local emissions in Beijing (59.6–79.5%) predominated the daily surface BC concentrations in severe haze days, followed by emissions in Hebei (12.7–24.2%) and outside BTH (4.1–13.7%), while emissions of these three regions were all important to the daily BC concentrations at the top of the PBL, by 35.9–61.9%, 23.7–39.1%, and 9.2–23.0%, respectively. Daily BC concentrations during haze events were most sensitive (89.8–99.3%) to sources on the severe haze days and also their previous 2 days. The contributions of local emissions in Beijing peaked on the pollution days and their previous one day. Emissions in Tianjin and Hebei and outside BTH showed the impact on timescale of 0–3 days and 0–5 days.

Our adjoint analyses of BC are important for understanding the sources and formation mechanisms of severe haze events in BTH and support a joint regional control policy for effectively mitigating the $PM_{2.5}$ air pollution. Targeted emission control measures can be implemented when the dominant synoptic weather patterns are predicted. Differences exist between observed and simulated BC as the uncertainties in model resolutions and emissions. Observation data assimilation would improve the model performance and hence BC source attribution. Future studies include assimilation of BC measurements using the adjoint model, such as surface and aircraft BC measurements, and aerosol absorption optical depths, which would be valuable for air quality forecasts and emission mitigation measures.

CRediT authorship contribution statement

Yu-Hao Mao: Conceptualization, Methodology, Writing - review & editing. **Xincheng Zhao:** Investigation, Formal analysis, Visualization. **Hong Liao:** Conceptualization. **Delong Zhao:** Data curation. **Ping Tian:** Data curation. **Daven K. Henze:** Methodology. **Hansen Cao:** Formal analysis. **Lin Zhang:** Formal analysis. **Jiandong Li:** Formal analysis. **Jing Li:** Data curation. **Liang Ran:** Data curation. **Qiang Zhang:** Data curation.

Declaration of Competing interest

The authors declare that they have no known competing financial interests or personal relationships that could have appeared to influence the work reported in this paper.

Acknowledgment

This work was supported by the National Natural Science Foundation of China (41605117), the National Key Research and Development Program of China (2016YFA0602001), and the China Postdoctoral Science Foundation (2017M620218, 2018T110526). HC and DKH recognize support from NASA (80NSSC18K0689, NNX16AQ26G). The GEOS-Chem model is managed by the Atmospheric Chemistry Modeling group at Harvard University with support from the NASA ACMAP program.

Appendix A. Supplementary data

Supplementary data to this article can be found online at https://doi.org/10.1016/j.scitotenv.2020.140149.

References

Anenberg, S.C., Talgo, K., Arunachalam, S., Dolwick, P., Jang, C., West, J.J., 2011. Impacts of global, regional, and sectoral black carbon emission reductions on surface air quality and human mortality. Atmos. Chem. Phys. 11, 7253–7267.

Anenberg, S.C., Schwartz, J., Shindell, D., Amann, M., Faluvegi, G., Klimont, Z., Janssens-Maenhout, G., Pozzoli, L., Van Dingenen, R., Vignati, E., Emberson, L., Muller, N.Z., West, J.J., Williams, M., Demkine, V., Hicks, W.K., Kuylenstierna, J., Raes, F., Ramanathan, V., 2012. Global air quality and health co-benefits of mitigating near-term climate change through methane and black carbon emission controls. Environ. Health Persp. 120 (6), 831–839.

Bey, I., Jacob, D.J., Yantosca, R.M., Logan, J.A., Field, B.D., Fiore, A.M., Li, Q., Liu, H.Y., Mickley, L.J., Schultz, M.G., 2001. Global modeling of tropospheric chemistry with assimilated meteorology: model description and evaluation. J. Geophys. Res. Atmos. 106 (D19), 23073–23095. https://doi.org/10.1029/2001JD000807.

Bond, T.C., Doherty, S.J., Fahey, D.W., Forster, P.M., Berntsen, T., DeAngelo, B.J., Flanner, M.G., Ghan, S., Kärcher, B., Koch, D., Kinne, S., Kondo, Y., Quinn, P.K., Sarofim, M.C., Schultz, M.G., Schulz, M., Venkataraman, C., Zhang, H., Zhang, S., Bellouin, N., Guttikunda, S.K., Hopke, P.K., Jacobson, M.Z., Kaiser, J.W., Klimont, Z., Lohmann, U., Schwarz, J.P., Shindell, D., Storelvmo, T., Warren, S.G., Zender, C.S., 2013. Bounding the role of black carbon in the climate system: scientific assessment. J. Geophys. Res. Atmos. 118 (11), 5380–5552.

Cai, W.J., Li, K., Liao, H., Wang, H.J., Wu, L.X., 2017. Weather conditions conducive to Beijing severe haze more frequent under climate change. Nat. Clim. Chang. 7, 257–262.

Chang, L., Li, J., Li, C., Tan, W., Tian, X., Xu, X. Seasonal and diurnal variability of aerosol optical properties at an urban location in Beijing China. Submitted to Environ. Pollut..

Chen, H., Li, J., Ge, B., Yang, W., Wang, Z., Huang, S., Wang, Y., Yan, P., Li, J., Zhu, L., 2015. Modeling study of source contributions and emergency control effects during a severe haze episode over the Beijing-Tianjin-Hebei area. Sci. China https://doi.org/10.1007/s11426-015-5458-y.

Chen, Y., Schleicher, N., Fricker, M., Cen, K., Liu, X.-L., Kaminski, U., Yu, Y., Wu, X.-F., Norra, S., 2016. Long-term variation of black carbon and PM2.5 in Beijing, China with respect to meteorological conditions and governmental measures. Environ. Pollut. 212, 269–278.

Ding, A.J., Huang, X., Nie, W., Sun, J.N., Kerminen, V.-M., Petäjä, T., Su, H., Cheng, Y.F., Yang, X.-Q., Wang, M.H., Chi, X.G., Wang, J.P., Virkkula, A., Guo, W.D., Yuan, J., Wang, S.Y., Zhang, R.J., Wu, Y.F., Song, Y., Zhu, T., Zilitinkevich, S., Kulmala, M., Fu, C.B., 2016. Enhanced haze pollution by black carbon in megacities in China. Geophys. Res. Lett. 43, 2873–2879.

Fu, T.M., Cao, J.J., Zhang, X.Y., Lee, S.C., Zhang, Q., Han, Y.M., Qu, W.J., Han, Z., Zhang, R., Wang, Y.X., Chen, D., Henze, D.K., 2012. Carbonaceous aerosols in China: top-down constraints on primary sources and estimation of secondary contribution. Atmos. Chem. Phys. 12 (5), 2725–2746.

Henze, D.K., Hakami, A., Seinfeld, J.H., 2007. Development of the adjoint of GEOS-Chem. Atmos. Chem. Phys. 7, 2413–2433.

Henze, D.K., Seinfeld, J.H., Shindell, D.T., 2009. Inverse modeling and mapping US air quality influences of inorganic $PM_{2.5}$ precursor emissions using the adjoint of GEOS-Chem. Atmos. Chem. Phys. 9, 5877–5903.

Huth, R., 2000. A circulation classification scheme applicable in GCM studies. Theor. Appl. Climatol. 67, 1–2), 1–18.

Intergovernmental Panel on Climate Change (IPCC) Climate Change 2013, 2013. In: Stocker, T.F., Qin, D., Plattner, G.-K., Tignor, M., Allen, S.K., Boschung, J., Nauels, A., Xia, Y., Bex, V., Midgley, P.M. (Eds.), The Physical Science Basis. Contribution of Working Group I to the Fifth Assessment Report of the Intergovernmental Panel on Climate Change. Cambridge University Press, Cambridge, United Kingdom and New York, NY, USA (1535 pp).

Janssens-Maenhout, G., Crippa, M., Guizzardi, D., Dentener, F., Muntean, M., Pouliot, G., Keating, T., Zhang, Q., Kurokawa, J., Wankmüller, R., Denier van der Gon, H., Kuenen, J.J.P., Klimont, Z., Frost, G., Darras, S., Koffi, B., Li, M., 2015. HTAP_v2: a mosaic of regional and global emission grid maps for 2008 and 2010 to study hemispheric transport of air pollution. Atmos. Chem. Phys. 15, 11411–11432.

Jin, J., Yan, P., Ma, Z., Lin, W., Liu, N., Ma, J., Zhang, X., Jia, X., 2014. Characteristics of PM2.5 in Beijing and surrounding areas from January to March in 2013. J. of Appl. Meteor. Sci. 25 (6), 690–700.

Kopacz, M., Mauzerall, D.L., Wang, J., Leibensperger, E.M., Henze, D.K., Singh, K., 2011. Origin and radiative forcing of black carbon transported to the Himalayas and Tibetan Plateau. Atmos. Chem. Phys. 11 (6), 2837–2852.

Li, K., Liao, H., Mao, Y.H., Ridley, D.A., 2016. Sectoral and regional contributions to black carbon and its direct radiative forcing in China. Atmos. Environ. 124, 351–366.

Li, J., Yang, W., Wang, Z., Chen, H., Hua, B., Li, J., Sun, Y., Fu, P., Zhang, Y., 2016. Modeling study of surface ozone source-receptor relationships in East Asia. Atmos. Environ. 167, 77–88.
Li, K., Liao, H., Cai, W.J., Yang, Y., 2018. Attribution of anthropogenic influence on atmospheric patterns conducive to recent most severe haze over eastern China. Geophys. Res. Lett. 45 (4), 2072–2081.
Li, J., Liao, H., Hu, J., Li, N., 2019. Severe particulate pollution days in China during 2013-2018 and the associated typical weather patterns in Beijing-Tianjin-Hebei and the Yangtze River Delta regions. Environ. Pollut. 248, 74–81.
Liao, L., Liao, H., 2014. Role of the radiative effect of black carbon in simulated $PM_{2.5}$ concentrations during a haze event in China. Atmos. Oceanic Sci. Lett. 7 (5), 434–440.
Liu, D., Quennehen, B., Darbyshire, E., Allan, J.D., Williams, P.I., Taylor, J.W., Bauguitte, S.J.-B., Flynn, M.J., Lowe, D., Gallagher, M.W., Bower, K.N., Choularton, T.W., Coe, H., 2015. The importance of Asia as a source of black carbon to the European Arctic during springtime 2013. Atmos. Chem. Phys. 15, 11537–11555.
Liu, M., Song, Y., Yao, H., Kang, Y., Li, M., Huang, X., Hu, M., 2015. Estimating emissions from agricultural fires in the North China Plain based on MODIS fire radiative power. Atmos. Environ. 112, 326–334.
Lu, Z., Zhang, Q., Streets, D.G., 2011. Sulfur dioxide and primary carbonaceous aerosol emissions in China and India, 1996-2010. Atmos. Chem. Phys. 11 (18), 9839–9864.
Lu, Z., Streets, D.G., Zhang, Q., Wang, S., 2012. A novel back-trajectory analysis of the origin of black carbon transported to the Himalayas and Tibetan plateau during 1996-2010. Geophys. Res. Lett. 39 (1).
Mao, Y.H., Li, Q.B., Henze, D.K., Jiang, Z., Jones, D.B.A., Kopacz, M., He, C., Qi, L., Gao, M., Hao, W.-M., Liou, K.-N., 2015. Estimates of black carbon emissions in the western United States using the GEOS-Chem adjoint model. Atmos. Chem. Phys. 15, 7685–7702.
Mao, Y.H., Liao, H., Han, Y., Cao, J., 2016. Impacts of meteorological parameters and emissions on decadal and interannual variations of black carbon in China for 1980–2010. J. Geophys. Res. Atmos. 121, 1822–1843.
Mao, Y.H., Liao, H., Chen, H.S., 2017. Impacts of East Asian summer and winter monsoons on interannual variations of mass concentrations and direct radiative forcing of black carbon over eastern China. Atmos. Chem. Phys. 17, 4799–4816.
Miao, Y.C., Guo, J.P., Liu, S.H., Liu, H., Li, Z.Q., Zhang, W.C., Zhai, P.M., 2017. Classification of summertime synoptic patterns in Beijing and their associations with boundary layer structure affecting aerosol pollution. Atmos. Chem. Phys. 17, 3097–3110.
Qi, L., Li, Q., Henze, D. K., Tseng, H,-L., He, C., 2017. Sources of springtime surface black carbon in the Arctic: an adjoint analysis for April 2008. Atmos. Chem. Phys. 17, 9697–9716.
Qin, Y., Xie, S.D., 2012. Spatial and temporal variation of anthropogenic black carbon emissions in China for the period 1980-2009. Atmos. Chem. Phys. 12 (11), 4825–4841.
Ramanathan, V., Carmichael, G., 2008. Global and regional climate changes due to black carbon. Nat. Geosci. 1, 221–227.
Ran, L., Deng, Z.Z., Wang, P.C., Xia, X.A., 2016. Black carbon and wavelength-dependent aerosol absorption in the North China Plain based on two-year aethalometer measurements. Atmos. Environ. 142, 132–144.
Shindell, D., Kuylenstierna, J.C.I., Vignati, E., van Dingenen, R., Amann, M., Klimont, Z., Anenberg, S.C., Muller, N., Janssens-Maenhout, G., Raes, F., Schwartz, J., Faluvegi, G., Pozzoli, L., Kupiainen, K., Höglund-Isaksson, L., Emberson, L., Streets, D., Ramanathan, V., Hicks, K., Oanh, N.T.K., Milly, G., Williams, M., Demkine, V., Fowler, D., 2012. Simultaneously mitigating near-term climate change and improving human health and food security. Science 335 (6065), 183–189.
Smith, K.R., Jerrett, M., Anderson, H.R., Burnett, R.T., Stone, V., Derwent, R., Atkinson, R.W., Cohen, A., Shonkoff, S.B., Krewski, D., Pope III, C.A., Thun, M.J., Thurston, G., 2009. Public health benefits of strategies to reduce greenhouse-gas emissions: health implications of short-lived greenhouse pollutants. Lancet 374, 2091–2103.
Song, C.B., Wu, L., Xie, Y.C., He, J.J., Chen, X., Wang, T., Lin, Y.C., Jin, T.S., Wang, A.X., Liu, Y., Dai, Q.L., Liu, B.S., Wang, Y.N., Mao, H.J., 2017. Air pollution in China: status and spatiotemporal variations. Environ. Pollut. 227, 334–347.
van der Werf, G.R., Randerson, J.T., Giglio, L., van Leeuwen, T.T., Chen, Y., Rogers, B.M., Mu, M., van Marle, M.J.E., Morton, D.C., Collatz, G.J., Yokelson, R.J., Kasibhatla, P.S., 2017. Global fire emissions estimates during 1997–2016. Earth Syst. Sci. Data 9, 697–720.
Wang, R., Tao, S., Wang, W., Liu, J., Shen, H., Shen, G., Wang, B., Liu, X., Li, W., Huang, Y., Zhang, Y., Lu, Y., Chen, H., Chen, Y., Wang, C., Zhu, D., Wang, X., Li, B., Liu, W., Ma, J., 2012. Black carbon emissions in China from 1949 to 2050. Environ. Sci. Technol. 46 (14), 7595–7603.
Wang, L.T., Wei, Z., Yang, J., Zhang, Y., Zhang, F.F., Su, J., Meng, C.C., Zhang, Q., 2014. The 2013 severe haze over southern Hebei, China: model evaluation, source apportionment, and policy implications. Atmos. Chem. Phys. 14, 3151–3173.
Wang, Y.G., Ying, Q., Hu, J.L., Zhang, H.L., 2014. Spatial and temporal variations of six criteria air pollutants in 31 provincial capital cities in China during 2013–2014. Environ. Int. 73, 413–422.
Wang, Y., Zhang, Q., Jiang, J., Zhou, W., Wang, B., He, K., Duan, F., Zhang, Q., Philip, Q., Xie, Y., 2014. Enhanced sulfate formation during China's severe winter haze episode in January 2013 missing from current models. J. Geophys. Res. 119, 10425–10440.
Wang, S.X., Zhao, B., Cai, S.Y., Klimont, Z., Nielsen, C.P., Morikawa, T., Woo, J.H., Kim, Y., Fu, X., Xu, J.Y., Hao, J.M., He, K.B., 2014. Emission trends and mitigation options for air pollutants in East Asia. Atmos. Chem. Phys. 14, 6571–6603.
Wang, M., Xu, B., Cao, J., Tie, X., Wang, H., Zhang, R., Qian, Y., Rasch, P.J., Zhao, S., Wu, G., Zhao, H., Joswiak, D.R., Li, J., Xie, Y., 2015. Carbonaceous aerosols recorded in a southeastern Tibetan glacier: analysis of temporal variations and model estimates of sources and radiative forcing. Atmos. Chem. Phys. 15, 1191–1204.
Wang, Y., Foy, de B., Schauer, J.J., Olson, R.M., Zhang, Y., Li, Z., Zhang, Y., 2017. Impacts of regional transport on black carbon in Huairou, Beijing, China. Environ. Pollut. 221, 75–84.
Wang, J.D., Zhao, B., Wang, S.X., Yang, F.M., Xing, J., Morawska, L., Ding, A.J., Kulmala, M., Kerminen, V.M., Kujansuu, J., Wang, Z.F., Ding, D., Zhang, X.Y., Wang, H.B., Tian, M., Petaja, T., Jiang, J.K., Hao, J.M., 2017. Particulate matter pollution over China and the effects of control policies. Sci. Total Environ. 426–447.
Wendisch, M., Hellmuth, O., Ansmann, A., Heintzenberg, J., Engelmann, R., Althausen, D., Eichler, H., Müller, D., Hu, M., Zhang, Y., Mao, J., 2008. Radiative and dynamic effects of absorbing aerosol particles over the Pearl River Delta, China. Atmos. Environ. 42, 6405–6416.
Wu, Y., Zhang, R., Tian, P., Tao, J., Hsu, S.-C., Yan, P., Wang, Q., Cao, J., Zhang, X., Xia, X., 2016. Effect of ambient humidity on the light absorption amplification of black carbon in Beijing during January 2013. Atmos. Environ. 124, 217–223.
Xu, J.M., Chang, L.Y., Qu, Y.H., Yan, F.X., Wang, F.Y., Fu, Q.Y., 2016. The meteorological modulation on $PM_{2.5}$ interannual oscillation during 2013 to 2015 in Shanghai, China. Sci. Total Environ. 572, 1138–1149.
Yang, Y., Wang, H., Smith, J.S., Ma, P.-L., Rasch, J.P., 2017. Source attribution of black carbon and its direct radiative forcing in China. Atmos. Chem. Phys. 17, 4319–4336.
Yin, L., Du, P., Zhang, M., Liu, M., Xu, T., Song, Yu, 2019. Estimation of emissions from biomass burning in China (2003–2017) based on MODIS fire radiative energy data. Biogeosciences 16, 1629–1640.
Zhang, Y.L., Cao, F., 2015. Fine particulate matter ($PM_{2.5}$) in China at a city level. Sci. Rep. 5, 14884.
Zhang, Q., Streets, D.G., Carmichael, G.R., He, K.B., Huo, H., Kannari, A., Klimont, Z., Park, I.S., Reddy, S., Fu, J.S., Chen, D., Duan, L., Lei, Y., Wang, L.T., Yao, Z.L., 2009. Asian emissions in 2006 for the NASA INTEX-B mission. Atmos. Chem. Phys. 9 (14), 5131–5153.
Zhang, X.Y., Wang, Y.Q., Niu, T., Zhang, X.C., Gong, S.L., Zhang, Y.M., Sun, J.Y., 2012. Atmospheric aerosol compositions in China: spatial/temporal variability, chemical signature, regional haze distribution and comparisons with global aerosols. Atmos. Chem. Phys. 12, 779–799.
Zhang, J.P., Zhu, T., Zhang, Q.H., Li, C.C., Shu, H.L., Ying, Y., Dai, Z.P., Wang, X., Liu, X.Y., Liang, A.M., Shen, H.X., Yi, B.Q., 2012. The impact of circulation patterns on regional transport pathways and air quality over Beijing and its surroundings. Atmos. Chem. Phys. 12, 5031–5053.
Zhang, R., Jing, J., Tao, J., Hsu, S.C., Wang, G., Cao, J., Lee, C.S.L., Zhu, L., Chen, Z., Zhao, Y., Shen, Z., 2013. Chemical characterization and source apportionment of PM2.5 in Beijing: seasonal perspective. Atmos. Chem. Phys. 13, 7053–7074.
Zhang, L., Liu, L., Zhao, Y., Gong, S., Zhang, X., Henze, D.K., Capps, S.L., Fu, T.-M., Zhang, Q., 2015. Source attribution of particulate matter pollution over North China with the adjoint method. Environ. Res. Lett. 10, 084011. https://doi.org/10.1088/1748-9326/10/8/084011.
Zhang, X., Rao, R., Huang, Y., Mao, M., Berg, M.J., Sun, W., 2015. Black carbon aerosols in urban Central China. J. of Quant. Spectrosc. Radiat. Transfer 150, 3–11.
Zhang, Y., Ding, A., Mao, H., Nie, W., Zhou, D., Liu, L., Huang, X., Fu, C., 2016. Impact of synoptic weather patterns and inter-decadal climate variability on air quality in the North China Plain during 1980–2013. Atmos. Environ. 124, 119–128.
Zhang, L., Shao, J., Lu, X., Zhao, Y., Hu, Y., Henze, D.K., Liao, H., Gong, S., Zhang, Q., 2016. Sources and processes affecting fine particulate matter pollution over North China: an adjoint analysis of the Beijing APEC period. Environ. Sci. Technol. 50 (16), 8731–8740.
Zheng, B., Tong, D., Li, M., Liu, F., Hong, C., Geng, G., Li, H., Li, X., Peng, L., Qi, J., Yan, L., Zhang, Y., Zhao, H., Zheng, Y., He, K., Zhang, Q., 2018. Trends in China's anthropogenic emissions since 2010 as the consequence of clean air actions. Atmos. Chem. Phys. 18, 14095–14111.
Zheng, H., Kong, S., Wu, F., Cheng, Y., Niu, Z., Zheng, S., Yang, G., Yao, L., Yan, Q., Wu, J., Zheng, M., Chen, N., Xu, K., Yan, Y., Liu, D., Zhao, D., Zhao, T., Bai, Y., Li, S., Qi, S., 2019. Intra-regional transport of black carbon between the south edge of the North China Plain and central China during winter haze episodes. Atmos. Chem. Phys. 19, 4499–4516.